Correction

APPLIED BIOLOGICAL SCIENCES, ENGINEERING

Correction for "High-throughput screening of rare metabolically active tumor cells in pleural effusion and peripheral blood of lung cancer patients," by Yin Tang, Zhuo Wang, Ziming Li, Jungwoo Kim, Yuliang Deng, Yan Li, James R. Heath, Wei Wei, Shun Lu, and Qihui Shi, which appeared in issue 10, March 7, 2017, of Proc Natl Acad Sci USA (114:2544–2549; first published February 21, 2017; 10.1073/pnas.1612229114).

The authors note that the affiliation for Yin Tang, Zhuo Wang, Yuliang Deng, and Qihui Shi should instead appear as Key Laboratory of Systems Biomedicine (Ministry of Education), Shanghai Center for Systems Biomedicine, Shanghai Jiao Tong University, Shanghai, 200240, China.

The authors also note that the affiliation for Ziming Li and Shun Lu should instead appear as Shanghai Lung Cancer Center, Shanghai Chest Hospital, Shanghai Jiao Tong University, Shanghai, 200030, China.

The corrected author and affiliation lines appear below. The online version has been corrected.

Yin Tang[a,1], Zhuo Wang[a,1], Ziming Li[b,1], Jungwoo Kim[c,d], Yuliang Deng[a], Yan Li[e], James R. Heath[c,d,f], Wei Wei[c,f,2], Shun Lu[b,2], and Qihui Shi[a,2]

[a]Key Laboratory of Systems Biomedicine (Ministry of Education), Shanghai Center for Systems Biomedicine, Shanghai Jiao Tong University, Shanghai, 200240, China; [b]Shanghai Lung Cancer Center, Shanghai Chest Hospital, Shanghai Jiao Tong University, Shanghai, 200030, China; [c]NanoSystems Biology Cancer Center, California Institute of Technology, Pasadena, CA 91125; [d]Division of Chemistry and Chemical Engineering, California Institute of Technology, Pasadena, CA 91125; [e]Shanghai Municipal Hospital of Traditional Chinese Medicine, Shanghai, 200071, China; and [f]Department of Molecular and Medical Pharmacology, David Geffen School of Medicine, University of California, Los Angeles, CA 90095

www.pnas.org/cgi/doi/10.1073/pnas.1703650114

CORRECTION

High-throughput screening of rare metabolically active tumor cells in pleural effusion and peripheral blood of lung cancer patients

Yin Tang[a,1], Zhuo Wang[a,1], Ziming Li[b,1], Jungwoo Kim[c,d], Yuliang Deng[a], Yan Li[e], James R. Heath[c,d,f], Wei Wei[c,f,2], Shun Lu[b,2], and Qihui Shi[a,2]

[a]Key Laboratory of Systems Biomedicine (Ministry of Education), Shanghai Center for Systems Biomedicine, Shanghai Jiao Tong University, Shanghai, 200240, China; [b]Shanghai Lung Cancer Center, Shanghai Chest Hospital, Shanghai Jiao Tong University, Shanghai, 200030, China; [c]NanoSystems Biology Cancer Center, California Institute of Technology, Pasadena, CA 91125; [d]Division of Chemistry and Chemical Engineering, California Institute of Technology, Pasadena, CA 91125; [e]Shanghai Municipal Hospital of Traditional Chinese Medicine, Shanghai, 200071, China; and [f]Department of Molecular and Medical Pharmacology, David Geffen School of Medicine, University of California, Los Angeles, CA 90095

Edited by Chad A. Mirkin, Northwestern University, Evanston, IL, and approved January 31, 2017 (received for review July 25, 2016)

Malignant pleural effusion (MPE), the presence of malignant cells in pleural fluid, is often the first sign of many cancers and occurs in patients with metastatic malignancies. Accurate detection of tumor cells in pleural fluid is crucial because the presence of MPE denotes an advanced stage of disease and directs a switch in clinical managements. Cytology, as a traditional diagnostic tool, has limited sensitivity especially when tumor cells are not abundant, and may be confounded by reactive mesothelial cells in the pleural fluid. We describe a highly sensitive approach for rapid detection of metabolically active tumor cells in MPE via exploiting the altered glucose metabolism of tumor cells relative to benign cells. Metabolically active tumor cells with high glucose uptake, as evaluated by a fluorescent glucose analog (2-NBDG), are identified by high-throughput fluorescence screening within a chip containing 200,000 addressable microwells and collected for malignancy confirmation via single-cell sequencing. We demonstrate the utility of this approach through analyzing MPE from a cohort of lung cancer patients. Most candidate tumor cells identified are confirmed to harbor the same driver oncogenes as their primary lesions. In some patients, emergence of secondary mutations that mediate acquired resistance to ongoing targeted therapies is also detected before resistance is manifested in the clinical imaging. The detection scheme can be extended to analyze peripheral blood samples. Our approach may serve as a valuable complement to cytology in MPE diagnosis, helping identify the driver oncogenes and resistance-leading mutations for targeted therapies.

pleural effusion | lung cancer | glucose uptake | diagnosis | CTC

Pleural effusion (PE) is associated with many types of malignancies, as exemplified by nonsmall cell lung cancer (NSCLC), breast cancer, Koposi sarcoma, and lymphomas (1). The accurate diagnosis of the etiology of the effusion, especially the identification of malignant tumor cells in the pleural fluid, is of great clinical significance for lung cancer patients, because the presence of malignant cells in PE denotes an advanced stage of disease with metastasis (M1a staging) and directs the patient management from curative intent to palliative care (2).

Cytological analysis by thoracentesis is a traditional and minimally invasive diagnostic tool of MPE (2). However, it suffers a low sensitivity of only ~60% because of the difficulties in the distinction among mesothelial, neoplastic, and reactive cells even for highly experienced pathologists (1). Although inclusion of immunohistochemistry (IHC) increases diagnostic sensitivity of MPE (3), no universal marker of malignancy exists and IHC staining based on a broad range of markers is time-consuming. Many malignant effusions are hemorrhagic with red blood cells and lymphocytes as predominant cell types (1). The number of tumor cells in the effusion is relatively small and even rare for patients who are in an early stage of metastasis or who have been treated with chemotherapies or targeted therapies, further challenging the accurate diagnosis of MPE with cytology.

Recent advancement in detection of rare circulating tumor cells (CTCs) in peripheral blood may present an opportunity to identify malignant cells in other body fluids, such as PE (4). However, most approaches available for detecting CTCs include an enrichment step and a subsequent immunostaining-based CTC identification. The enrichment step is generally based on epithelial marker isolation, white blood cell depletion, or discrimination of physical properties. The immunostaining-based CTC identification, first adopted by the CellSearch system, includes cell fixation, permeabilization, and staining with a mixture of anti-CD45 (common leukocyte marker), anti-cytokeratin (CK, epithelial marker), and DAPI (cell nucleus marker) to pinpoint epithelial cells in blood (5). Therefore, these approaches may not be directly adapted to obtain a definitive diagnosis of a malignant effusion, because they are incapable of distinguishing malignant tumor cells from benign epithelial cells and reactive mesothelial cells in PE that also express epithelial markers (5). The use of epithelial markers also intrinsically limits the diagnoses of pleural fluid of nonepithelial malignancies. Given the important clinical implications of MPE, a new approach that allows definitive diagnosis of malignant effusion through rapid

Significance

Identification of cancer cells in the pleural effusions of lung cancer patients is an important clinical diagnosis to verify the malignant pleural involvement. Elevated glucose uptake is a hallmark of cancer cells and has been used in positron-emission tomography to detect malignant tumors in vivo. We hypothesize that cells with enhanced glucose uptake and without expression of leukocyte markers in pleural effusion or peripheral blood samples are highly likely to be malignant cells that can be confirmed via single-cell sequencing. To this end, a high-throughput metabolic-based assay is developed for rapid detection of rare metabolically active tumor cells in pleural effusion, enabling sensitive diagnosis of malignant pleural effusion in the clinic that is associated with metastatic malignancies.

Author contributions: W.W., S.L., and Q.S. designed research; Y.T., Z.W., J.K., and Y.D. performed research; Z.L., Y.L., and S.L. contributed clinical samples; Y.T., Z.W., W.W., and Q.S. analyzed data; and J.R.H., W.W., and Q.S. wrote the paper.

The authors declare no conflict of interest.

This article is a PNAS Direct Submission.

Data deposition: The WES data reported in this paper have been deposited in the ArrayExpress database (accession no. E-MTAB-4948).

[1]Y.T., Z.W., and Z.L. contributed equally to this work.

[2]To whom correspondence may be addressed. Email: weiwei@mednet.ucla.edu, lushun@csco.org.cn, or qihuishi@sjtu.edu.cn.

This article contains supporting information online at www.pnas.org/lookup/suppl/doi:10.1073/pnas.1612229114/-/DCSupplemental.

www.pnas.org/cgi/doi/10.1073/pnas.1612229114

and accurate identification of malignant tumor cells in PE is greatly desired.

Here, we demonstrate an enrichment-free, metabolic-based approach for high-throughput screening of metabolically active tumor cell in PE samples via exploiting the innate difference in glucose uptake between malignant tumor cells and benign cells in lung cancer patients. Altered glucose metabolism is a hallmark of many cancers (6). The enhanced glucose uptake as a result of the glycolytic switch and elevated expression of glucose transporters (GLUTs) in most cancer cells has been used in positron-emission tomography (PET) to image malignant tumors in vivo. In NSCLC patients, enhanced glycolysis and glucose oxidation were observed in vivo for tumors relative to benign cells (7). ^{18}F-fluoro-2-deoxy-D-glucose (FDG) uptake has been found to correlate with tumor vitality with prognostic value in patient response (8). Therefore, we hypothesize that the quantitation of glucose uptake with fluorescent glucose analog 2-NBDG (9–12) combined with leukocyte marker CD45 staining presents an opportunity to functionally distinguish metabolically active malignant tumor cells from other nontumor cells in PE. With the aid of a microchip device with addressable microwells and a computerized high-speed fluorescent imaging system, this rapid functional assay enables high-throughput screening of a large number of cells at single cell resolution, leading to detection of putative metabolically active tumor cells in pleural fluid without enrichment. All cells assayed are addressable, and the candidate tumor cells with high glucose uptake will therefore be retrieved individually for single-cell sequencing to confirm their malignancy and reveal their targetable driver oncogenes.

Results

Working Principle and Validation of the Detection Platform. The detection of tumor cells in PE was performed in microwell chip platform that accommodates 400 numbered blocks (Fig. 1*A* and *SI Appendix*, Fig. S1) with 200,000 addressable microwells. The experimental procedure is simple (Fig. 1*B*). Briefly, RBCs were removed by an ammonium chloride-based lysis buffer, and all nucleated cells were resuspended in HBSS and labeled with a fluorescent anti-CD45 antibody. These cells were then applied onto the microwell chip, sitting in an array of addressable microwells (*SI Appendix*, Fig. S1), and incubated with a fluorescent glucose analog 2-NBDG and EthD-1 (fluorescent dead cell marker). After triple labeling with CD45/2-NBDG/EthD-1, the microwell chip was imaged by a computerized high-speed fluorescent microscope in three fluorescent colors (CD45, Cy5; 2-NBDG, FITC; EthD-1, TRITC) to capture ∼700 images (*SI Appendix*, Fig. S2) in less than 10 min. A computational algorithm analyzed the images and identified candidate tumor cells that are viable (EthD-1$^-$), CD45 negative, and exhibit high glucose uptake (2-NBDG^{high}), followed by reviewing via experienced technicians. Once confirmed, the putative single tumor cells were retrieved by an automatic micromanipulator sequentially based on recorded addresses at a rate of 1 min per cell for single-cell sequencing that serves as a main control for confirmation of the malignancy of identified cells.

2-NBDG is a fluorescent analog of D-glucose that follows a similar metabolic pathway inside the cell. Prior work has shown that 2-NBDG enters a cell via glucose transporters and is phosphorylated at the C-6 position by hexokinases I–II. The phosphorylated fluorescent metabolite, 2-NBDG-6-phosphate, remains in the cell until decomposition into a nonfluorescent form (9–13). Compared with nonmalignant cells, 2-NBDG is rapidly taken up by malignant cells, providing an optical marker for detection of malignant cells. As a proof-of-concept demonstration, we treated A549 (an NSCLC cell line) cells with 2-NBDG (Fig. 1*C*) and compared their signal against CD45-labeled nucleated cells taken from three healthy donors' blood samples. Briefly, cells in the microwells were deprived of glucose for 10 min and then exposed to 0.4 mM 2-NBDG and 4 μM EthD-1 for 20 min at 37 °C. After extensive washing with cold PBS, the fluorescence signals of 2-NBDG, CD45, and EthD-1

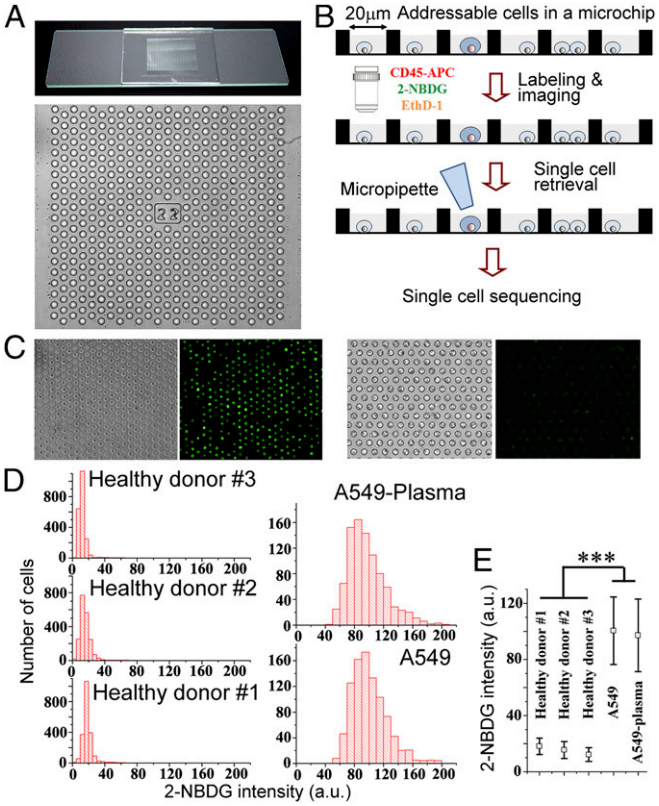

Fig. 1. The microwell chip and the working principle. (*A*) A microwell chip has 200,000 microwells with a diameter and the height of 25 μm and 20 μm, respectively. (*B*) The working flow of the enrichment-free tumor cell detection based on 2-NBDG uptake and CD45 expression. EthD-1$^-$/CD45$^-$/2-NBDG^{high} cells are identified as candidate tumor cells. (*C*) Bright field and fluorescent images of A549 cells and leukocytes sitting in microwells of the chip after treating with 2-NBDG. (*D, Left*) Histograms of 2-NBDG uptake in nucleated cells taken from three healthy donors' blood samples. (*D, Right*) Histograms of 2-NBDG uptake of A549 cells suspended in HBSS or healthy donor's plasma. (*E*) Comparison of 2-NBDG uptake between nucleated cells in healthy donor's blood samples and tumor cell line A549. Statistical significance was evaluated by Student's *t* test (two-tailed ***$P < 0.0001$).

were measured for all the cells at single cell resolution. The histograms of 2-NBDG uptakes are shown in Fig. 1*D*, in which a clear separation between leukocytes and tumor cells supports the feasibility of functionally discriminating metabolically active tumor cells from leukocytes with 2-NBDG uptake (Fig. 1*E*). Similar clear separation is also observed in the single-cell PET assay, in which FDG, the radioactive glucose analog, was used to quantitate glucose uptake of tumor cells and leukocytes (*SI Appendix*, Fig. S3). Therefore, 2-NBDG is consistent with FDG in quantifying in vitro glucose uptake of cells.

Identification of Metabolically Active Tumor Cells in PE Samples of Lung Cancer Patients. After validation of our detection scheme with lung cancer cell line, we tested the utility of our platform in the PE samples from a cohort of NSCLC patients (*SI Appendix*, Table S1). Briefly, approximately 500,000 nucleated cells labeled with allophycocyanin (APC)-conjugated anti-CD45 antibody were collected from each patient PE sample and applied onto a microwell chip. Following the protocol previously described, we identified putative metabolically active tumor cells with elevated glucose uptake interspersed in a high background of other nucleated cells presented in the PE, and retrieved them for single-cell sequencing. To ensure the majority of candidate cells are real tumor cells, we adapted the average 2-NBDG uptake of A549 cells (fluorescence intensity ∼100) as the cutoff value for

metabolically active cells. As shown below, among all of the patient PE samples tested, no leukocyte has 2-NBDG uptake higher this cutoff value.

Fig. 2*A* shows representative images of candidate tumor cells that are viable, CD45 negative, and exhibit high uptake of 2-NBDG (*SI Appendix*, Fig. S4) from the PE samples of patient 1. The histograms of 2-NBDG uptake in two typical blocks are shown in Fig. 2*B* and presented in three distinct subpopulations. Viable leukocytes (EthD-1$^-$/CD45$^+$) in the PE sample were found to mostly exhibit low uptake of 2-NBDG with a small number of cells exhibiting elevated uptake that was fewer than 100. Dead cells (EthD-1$^+$) also showed a low unspecific background of 2-NBDG because of the diffusion of the 2-NBDG molecules through the compromised cell membranes. In the CD45$^-$ cells, observations of low 2-NBDG signal were potentially from nonmalignant epithelial cells and mesothelial cells (*SI Appendix*, Fig. S5) present in the PE (1). In 1 mL of this PE sample, a total of five metabolically active candidate tumor cells were identified based on the criteria of EthD-1$^-$/CD45$^-$/2-NBDG$^{>100}$ and then retrieved sequentially for single-cell sequencing of a small panel of oncogenes (*EGFR, KRAS, PIK3CA, BRAF, TP53*) listed in *SI Appendix*, Table S2 (*SI Appendix*, Fig. S6). We identified a G12C missense mutation at codon 12 in exon 2 of *KRAS*, from a glycine to a cysteine (GGT > TGT) in three of five candidate tumor cells (Fig. 2*C* and *SI Appendix*, Table S3). The detected mutation was consistent with the mutation status found in the primary lesion of the patient (*SI Appendix*, Table S1). The three cells harboring *KRAS* mutation are therefore indeed tumor cells, confirming the malignant involvement of PE for patient 1, who was diagnosed as MPE by traditional cytology (Table 1).

To further resolve the mutational profile of the three cells with *KRAS* mutation and determine the malignancy of the other two cells, we performed the whole exome sequencing (WES) on these five putative cells. We screened the mutations with the Qiagen's Lung Cancer Panel, containing 45 most relevant driver oncogenes and tumor suppressor genes in lung cancer. A total of 26, 30, 23, 26, and 26 of 45 mutant genes are detected in cell 1 (mutant *KRAS*), cell 2 (mutant *KRAS*), cell 3 (wild-type *KRAS*), cell 4 (wild-type *KRAS*), and cell 5 (mutant *KRAS*), respectively. For all five cells, the number of nonsynonymous somatic mutations and small insertions and deletions (INDELs) of the 45 genes is shown in *SI Appendix*, Table S4 and Dataset S1, demonstrating a high mutational frequency in these critical driver oncogenes. Cells 3 and 4, while with wild-type *KRAS*, harbored missense mutations in the genes including *BRAF*, *EGFR*, *PIK3CA*, *PTEN*, and *TP53*, and showed similarity with the other three *KRAS* mutant tumor cells in the hierarchical clustering (Fig. 2*D*), indicating a high chance of malignancy of these two cells. As a result, all five metabolically active EthD-1$^-$/CD45$^-$/2-NBDG$^{>100}$ cells present in this PE sample were found to be either harboring the same mutant *KRAS* as the primary tumor or having high mutational frequency in other driver oncogenes, reassuring the validity of using glucose uptake as a metabolic marker for pinpointing the candidate tumor cells.

In ~500,000 nucleated cells from the PE sample from patient 3, 8 cells were identified as candidate tumor cells (Fig. 2*E*). Single-cell sequencing at the target genes (*SI Appendix*, Table S3) further showed that six of eight cells have an in-frame deletion in exon 19 of *EGFR* (E746_A750Del) and five of these six

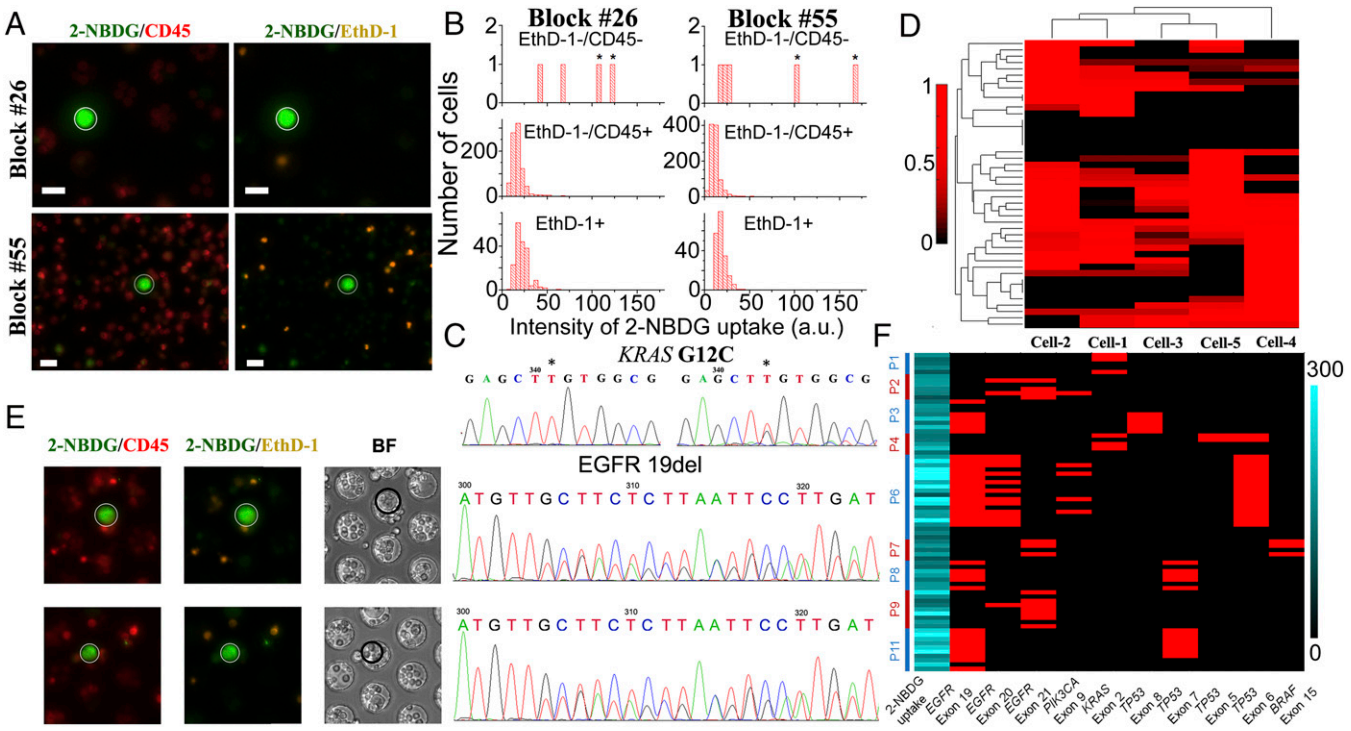

Fig. 2. Identification of tumor cells in pleural effusion samples. (*A*) Candidate tumor cells (circled) from patient 1 that are EthD-1$^-$/CD45$^-$/2-NBDG^{high}. (Scale bars: 25 μm.) (*B*) The histograms of 2-NBDG uptake from two typical blocks with three subpopulations, including EthD-1$^+$ cells (dead cells), EthD-1$^-$/CD45$^+$ cells (viable leukocytes), and EthD-1$^-$/CD45$^-$ cells. In these two blocks, four EthD-1$^-$/CD45$^-$/2-NBDG$^{>100}$ cells were identified as candidate tumor cells. (*C*) Single-cell Sanger sequencing results detected G12C missense mutation in exon 2 of *KRAS* from candidate tumor cells shown in *A*. (*D*) A clustering heat map of mutational frequency in 45 driver oncogenes and tumor suppressors from WES results of five candidate tumor cells. Note that the number of mutations of a gene was normalized to the largest number of missense mutation of that gene across the five cells. (Refer to *SI Appendix*, Table S4 for the list of genes). (*E*) Candidate tumor cells (circled) identified in PE sample from patient 3 with an in-frame deletion in exon 19 of EGFR. (*F*) Summary of 2-NBDG uptake and mutational profile of the putative tumor cells from patient PE samples. Each row represents the 2-NBDG uptake and target gene sequencing for each candidate tumor cell from the patient labeled at left. A red tile denotes a mutation in that gene, whereas a black tile denotes wild type (*SI Appendix*, Table S3).

Table 1. Comparison of our method to cytopathology and IHC results in MPE diagnosis

No.	Cytology of PE	IHC of PE	Our method on the same PE samples
1	MPE	TTF-1(+); P40(-); Napsin A(+); CK(+); CK7(+); Calretinin(–); CD45/LCA(–); GLUT-1(+); CEA(+)	MPE, $KRAS^{G12C}$
2	MPE	TTF-1(+); Calretinin(–); P40(–); CK(+); CD56(–)	MPE, $EGFR^{L858R}$, **$EGFR^{T790M}$**, **$PIK3CA^{E542K}$**
3	MPE	TTF-1(+); Napsin A(+); CK(+); VIM(-); Calretinin(–); D2-40(–); CK20(+); CK5/6(–); CK7(+); CD-X2(-)	MPE, $EGFR^{19del}$
4	MPE	TTF-1(-); Napsin A(-); CK(+); WT-1(–); Calretinin(–); D2-40(–); CEA(+); CD15($^{+/-}$); CK5/6(–); CK7(+)	*MPE*, $KRAS^{G12D}$, $KRAS^{G12V}$
6	MPE	TTF-1(+); Napsin A(+); CK(+); WT-1(–); Calretinin(–); D2-40(–); CEA(+); CK5/6(–); CK7(+)	MPE, $EGFR^{19del}$, **$EGFR^{T790M}$**, **$PIK3CA^{E545K}$**
7	UNSP	NA	MPE, $EGFR^{L858R}$, **$BRAF^{V600E}$**
8	MPE	TTF-1(+); WT-1(–); Calretinin($^{+/-}$); D2-40($^{+/-}$); GLUT-1(+); Napsin A($^{+/-}$)	MPE, $EGFR^{19del}$
9	UNSP	NA	MPE, $EGFR^{L858R}$, **$EGFR^{T790M}$**
10	UNSP	TTF-1(+); CK(+); WT-1(–); Calretinin(+); D2-40(–); CEA(+); GLUT-1(+); HBME-1(+) *	MPE, *ALK* fusion gene
11	MPE	TTF-1(+); Napsin A(-); WT-1(–); CK(+); Calretinin(–); D2-40(–); CK5/6(–); CK7(+); CEA(+);GLUT-1(+)	MPE, $EGFR^{19del}$
12–15	Benign PE	NA	Benign PE

Mutations on actionable oncogenes in bold are those resistant-leading secondary mutations different from primary tumors. CEA, carcinoembryonic antigen; D2-40, podoplanin; LCA, leucoyte common antigen, namely CD45; UNSP, unspecified; WT-1, Wilms tumor protein.
*IHC result of patient 10 was from biopsy of mediastinal lymph node rather than thoracentesis.

cells also have a $TP53^{R273H}$ mutation (CGT > CAT). The detected EGFR mutational status is consistent with the primary site of the tumor, confirming the malignancy of the effusion for this patient who has been concluded as MPE by cytology (Table 1). In the PE samples from patients 4, 6, 8, and 11, the same MPE screening assay was successfully performed with our approach (Fig. 2*F*, Table 1, and *SI Appendix*, Table S3). In patient 4, we found two types of tumor cells harboring $KRAS^{G12D}$ and $KRAS^{G12V}$ mutations, respectively, which is consistent with the mutational status found in the primary lesion of this patient. For patient 6, a total of 20 candidate tumor cells were picked out and 17 were found harboring the same $EGFR^{19del}$ (E746_A750Del) as the primary lesion (Fig. 2*F* and *SI Appendix*, Table S3). $EGFR^{T790M}$ mutation were also found in 12 of 17 tumor cells where some of them were simultaneously harboring $PIK3CA^{E545K}$ mutation as well (*SI Appendix*, Fig. S7). Both $EGFR^{T790M}$ and $PIK3CA^{E545K}$ mutations are reported to mediate acquired resistance to EGFR tyrosine kinase inhibitors (TKI) (14). Based on the clinical record, this patient received EGFR TKI therapy and later on developed resistance to it. She had not shown drug resistance in CT scans at the time of PE drawn. However, the emergence of resistance-leading mutations was clearly resolved via analyzing the metabolically active tumor cells in the PE sample. We also compared the glucose uptake against their cell sizes for the 17 malignant cells (*SI Appendix*, Fig. S8). No statistically significant correlation was identified between the cell size and the glucose uptake for these tumor cells. In the PE sample from patient 8, who received chemotherapy and targeted therapy (gefitinib), seven candidate tumor cells were identified and sequenced to harbor $EGFR^{19del}$ (E746_T751Del) mutation (Fig. 2*F* and *SI Appendix*, Table S3), whereas the primary tumor had both $EGFR^{19del}$ and $EGFR^{G719X}$ mutations (*SI Appendix*, Table S1). $EGFR^{G719X}$ mutation has been found to be associated with increased sensitivity to the EGFR TKIs including erlotinib and gefitinib (15, 16). The $EGFR^{G719X}$ mutant cells were therefore likely to be preferentially eliminated in the primary lesion by gefitinib and were not found in the PE sample of this patient. As negative controls, no metabolically active cells were identified in PE samples from noncancer patients 12–15 who have benign effusion (Table 1 and *SI Appendix*, Fig. S9).

Heterogeneous CK Expression in High Glucose Uptake Lung Cancer Cells. In the PE sample from patient 2 with an $EGFR^{L858R}$ mutation in his primary lesion, six cells were identified as candidate tumor cells (Fig. 3*A* and *SI Appendix*, Fig. S10). The sequencing results (*SI Appendix*, Table S3) showed that four cells have the consistent $EGFR^{L858R}$ mutation (CTG > CGG), and one cell has both $EGFR^{L858R}$ mutation and $PIK3CA^{E542K}$ mutation (GAA > AAA). $EGFR^{T790M}$ mutation is detected in two of six cells by an amplification refractory mutation system (ARMS) assay. The $EGFR^{T790M}$ and $PIK3CA^{E542K}$ mutations have been found to be associated with drug resistance of EGFR TKI (14). The sequencing results are consistent with the fact that the patient previously received the EGFR TKI therapy and started developing drug resistance at the time of PE drawn.

In addition to single-cell sequencing, this platform is also compatible to immunofluorescent staining to characterize the phenotype of the cells with high glucose uptake. In another PE sample of patient 2, following on-chip metabolic assay, cells in the microwells were fixed, permeablized, and immunostained with phycoerythrin-conjugated CK (PE-CK). After imaging and data analysis, candidate tumor cells were retrieved for single-cell sequencing at the exon 21 of *EGFR*, which has a known mutation of L858R. CD45$^-$/EthD-1$^-$/2-NBDG$^{>100}$ tumor cells with detected $EGFR^{L858R}$ mutation show heterogeneous CK expression (Fig. 3*B* and *SI Appendix*, Figs. S11 and S12), and only ~40% of these tumor cells are found to be CK positive, indicating an incompleteness in detection of tumor cells based solely on CK$^+$/CD45$^-$/DAPI$^+$ definition despite that it has been widely used in detecting rare epithelial tumor cells circulating in peripheral blood (17). A previous study on breast cancer patients where 50% of the HER2-amplified CTCs were found to be CK$^-$/CD45$^-$/DAPI$^+$ phenotype (18) echoes our observation. The absence of CK expression on tumor cells of epithelial origin may be attributed to epithelial-to-mesenchymal transition. Meanwhile, CK$^+$/2-NBDG^{low} cells harboring the tumor-specific $EGFR^{L858R}$ mutation were also found in the sample (*SI Appendix*, Fig. S11), which may be attributed to cell apoptosis.

Superior Performance in MPE Diagnosis Compared with Traditional Cytology. Our platform outperforms cytological and IHC approaches in two representative scenarios. The first one involves the inconclusive diagnosis of PE samples with traditional methods. For patient 10, initial cytological analysis found some suspicious cells in the PE but could not lead to a definitive diagnosis because it failed to determine the malignancy of those cells. In contrast, our platform identified five candidate metabolically active tumor cells from ~500,000 nucleated cells in the PE

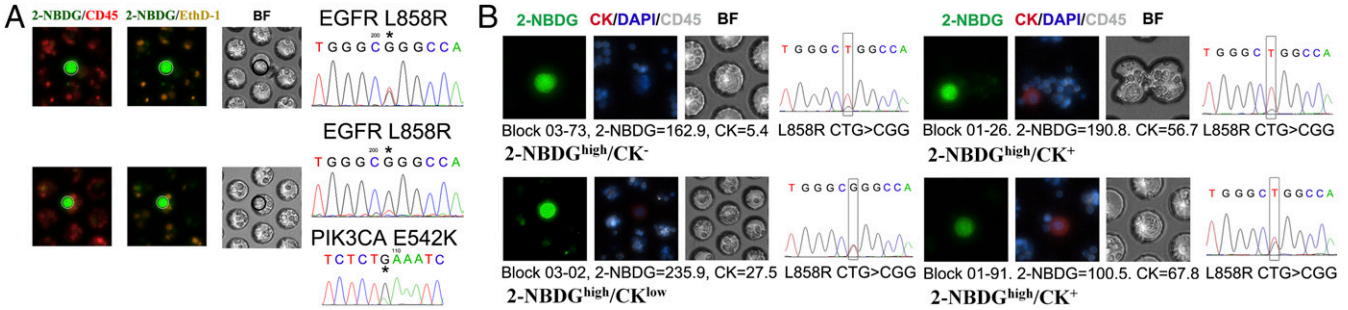

Fig. 3. CK expression in high glucose uptake tumor cells. (*A*) Representative images of candidate tumor cells (circled) identified in the PE sample from patient 2 with single-cell sequencing results showing the $EGFR^{L858}$ and $PIK3CA^{E542K}$ mutations. (*B*) Candidate tumor cells with $EGFR^{L858}$ mutation were stained with PE-CK and showed heterogeneous expression of CK.

sample of this patient. Single-cell sequencing showed that these cells are free of mutations in *EGFR*, *KRAS*, *BRAF*, and *PIK3CA* (*SI Appendix*, Table S3). However, transcriptome amplification of identified cells revealed the echinoderm microtubule-associated protein-like 4–anaplastic lymphoma kinase (*EML4-ALK*) fusion oncogene, which is consistent with the mutational status of the primary lesion, and the exclusive nature of the *EML4-ALK* rearrangement in NSCLC (19). In addition, immunostaining on the candidate tumor cells with thyroid transcription factor-1 (TTF-1) revealed a phenotype of $CD45^{-}/TTF\text{-}1^{+}/2\text{-}NBDG^{>100}$, indicating an origin of lung adenocarcinoma. These results lead to a conclusive malignant pleural involvement and are consistent with the IHC staining on the patient biopsy of mediastinal lymph node (Table 1).

The second scenario is related to MPE diagnosis for patients who are being treated with and respond to chemotherapy or targeted therapies. For these patients, tumor cells in the effusion serve as valuable resources for revealing any secondary mutations associated with the onset of therapy resistance in the clinic. However, the number of tumor cells present in the effusion is usually small and even rare after drug treatment, posing a significant technical challenge for cytology. For example, patient 7 with a primary tumor harboring $EGFR^{L858R}$ mutation received chemo- and EGFR TKI gefitinib initially (*SI Appendix*, Table S1). However, the tumor cells became resistant to gefitinib in less than 7 mo. The patient then received alectinib and AZD9191, an irreversible third-generation EGFR TKI. At the time of PE draw, cytological and IHC analyses failed to detect tumor cells in the effusion (Table 1). However, three candidate tumor cells were identified by our platform in the effusion from this patient and sequenced to harbor both $EGFR^{L858R}$ and $BRAF^{V600E}$ mutations (Fig. 2*F* and Table 1). The acquired $BRAF^{V600E}$ mutation was reported to be associated with decreased sensitivity to gefitinib (20), which may account for the rapid resistance development to gefitinib after an initial response.

Similarly, patient 9 with an $EGFR^{19del}$ in the primary tumor was treated with alectinib, an EGFR TKI (*SI Appendix*, Table S1). Cytological analysis failed to detect tumor cells in the PE sample drawn after the targeted therapy (Table 1). Our platform identified nine candidate tumor cells in the PE sample in which six of them harbor $EGFR^{L858R}$ mutation and one cell harbors both $EGFR^{L858R}$ and $EGFR^{T790M}$ mutations (Fig. 2*F* and *SI Appendix*, Fig. S13 and Table S3). The inconsistent mutational profiles between the primary tumor before targeted therapy and the tumor cells found in PE after therapy may be attributed to the tumor heterogeneity and clonal selection following the therapy. The emergence of secondary $EGFR^{T790M}$ mutations may imply an onset of resistance to alectinib in this patient.

Extension to the CTC Detection in Peripheral Blood Sample of Lung Cancer Patients. The enrichment-free, simple metabolic-based assay for identifying malignant cells in PE can be extended to detect rare tumor cells in other body fluids, such as CTCs in peripheral blood samples. In 1 mL of peripheral blood sample from patient 4, after lysis of RBCs, all nucleated cells were applied onto the microwell chip at a concentration of ~600,000 cells per chip. Two candidate CTCs were identified based on the $EthD\text{-}1^{-}/CD45^{-}/2\text{-}NBDG^{>100}$ criteria, and confirmed to be malignant cells bearing $KRAS^{G12D}$ mutation (Fig. 4), which is consistent with the mutational status found in PE and primary lesions (Table 1 and *SI Appendix*, Tables S1 and S3). Likewise, in 1 mL of peripheral blood sample from patient 3, eight candidate CTCs were identified and four of them were found harboring $EGFR^{19del}$ mutation, which is identical to the mutational status found in PE and primary lesions (Fig. 4*C*). We further challenged our detection scheme for identifying CTCs for patients at early clinical stage. In 1 mL of peripheral blood sample from patient 5 (stage Ib), three candidate CTCs were successfully identified and two of them were found harboring a $EGFR^{A864V}$ mutation (GCG > GTG) in exon 21, as shown in Fig. 4 *B* and *C*.

Discussion

The accurate evaluation of PE is critical in the clinic because it directs the staging and clinical managements of lung cancer patients. Pleural thoracentesis followed by the cytological analysis is the least invasive approach for diagnosing MPE in the clinic. Unfortunately, this approach has a large variation in sensitivity depending on the fluid amount and quality, and the experience of the cytopathologists (21). The existence of mesothelial cells with atypical nuclear changes that resemble the malignant cells further elevates the diagnostic threshold and confounds the sensitivity of cytology. As a representative scenario in the clinic, lung cancer patients with early stage metastasis often have a positive chest computed tomography (CT) scan for lung lesions, but a negative or inconclusive diagnosis for MPE because the cytopathological analysis is insensitive to MPE samples with rare

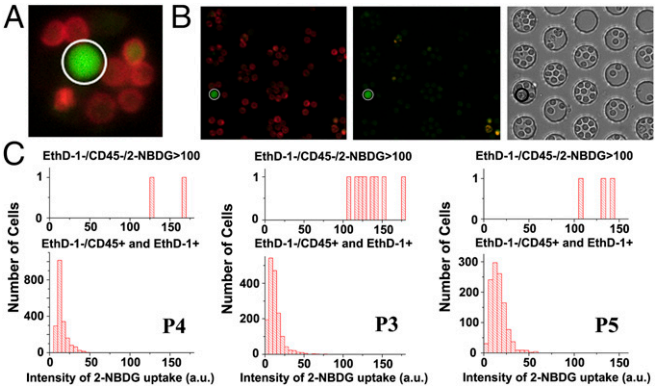

Fig. 4. Representative fluorescence images of CTCs (circled) identified in peripheral blood samples from patient 4 (*A*) and patient 5 (*B*). (*C*) Histograms of 2-NBDG uptake for blood samples of patients 3, 4, and 5.

tumor cells interspersed in a large number of blood cells (22). In this case, pleural biopsy or thoracoscopic surgery will normally be indicated for more accurate evaluation of malignant pleural involvement and metastasis. However, these invasive approaches require general anesthesia and may induce significant patient morbidity and increased health care costs and, thus, sometimes are not a good option for patients with advanced-stage disease (23).

Motivated by these clinical challenges, we have developed a metabolic-based high-throughput screening approach to rapidly identify rare tumor cells at single cell resolution in a high background of leukocytes, followed by single-cell sequencing for confirmation of malignancy and identification of targetable driver oncogenes. In contrast to the cytological diagnosis of MPE that normally requires more than 50 mL of effusion (24), this strategy is capable to detect rare malignant tumor cells in less than 1 mL of effusion fluid. Therefore, it can potentially be extended to detect CTCs in peripheral blood because that has already been demonstrated in patients 3, 4, and 5, given the utility of this approach for blood analysis requires more comprehensive evaluation in statistical number of patients.

High glucose-uptake tumor cells represent a metabolically active subset of viable tumor cells present in PE or peripheral blood (25). These tumor cells are prone to being more glycolytic and, therefore, might have the potential to seed metastasis or home to primary tumor sites. It has been shown that glucose uptake of malignant cells in PE is an independent prognostic indicator in NSCLC (26). More work is ongoing to validate the clinical relevance and therapeutic importance of this metabolically active subset. In this study, we set a high threshold (2-NBDG > 100) for discriminating leukocytes and tumor cells, aiming to ensure most candidate cells for sequencing are tumor cells. The successful detection of malignant tumor cells in all MPE samples where no leukocyte has 2-NBDG uptake of more than 100 further supports the validity of this cutoff value in our system. It is worthwhile to note that the optimal cutoff value of 2-NBDG is system-specific, depending on the tumor type under study, the processing and staining protocols, and the instrumental settings, and needs to be redetermined when working on a new system. Importantly, the storage and shipping of PE and peripheral blood samples may compromise the viability of tumor cells and, therefore, induce a decrease in glucose uptake. All samples should be processed and characterized immediately after collection from patients.

Given its capability of identifying rare tumor cells in minimal amount of PE and its feasibility of implementing a standardized and automatable assay protocol, our detection platform has the potential to be used in conjunction with traditional cytology in the clinic to provide a more sensitive assessment when cytology alone fails to provide a definitive diagnosis of MPE (Table 1). It is beneficial to patients with early stage metastasis and inconclusive MPE diagnoses where a reassessment by our approach could potentially release them from more invasive interventions (as patient 10). In addition, both our data and the data published elsewhere (27) have shown a high concordance rate of mutational profile between tumor cells in MPEs and primary tumor specimens for NSCLC patients. Therefore, our approach offers a minimally invasive means for resolving targetable mutations at single cell resolution, when the mutational profile of the primary tumor site is not available for a patient (as patient 5), which is frequently encountered in the clinic (28, 29). Furthermore, patients are more likely to accept repeated thoracentesis rather than rebiopsy of the primary tumor to detect molecular changes (27), which makes our detection approach promising in monitoring the change in mutational profile and the emergence of any secondary mutations at the onset of resistance during targeted therapies. Of course, these utilities require extensive prospective or retrospective validations on clinical samples first, and our work sets a stage for such clinical studies in the future.

Materials and Methods

PE and blood samples were obtained from lung cancer patients in Shanghai Chest hospital and Shanghai Municipal Hospital of Traditional Medicine with informed consent. The experimental protocols have been approved by Ethics and Scientific Committees of both hospitals. Please refer to *SI Appendix, SI Materials and Methods* for cell lines and reagents used, microwell chip fabrication, and protocols for tumor cell identification and sequencing.

ACKNOWLEDGMENTS. We thank the following agencies and foundations for support: National Natural Science Foundation of China Grants 81373621 (to Q.S.) and 81401880 (to S.L.) and Shanghai Scientific Research Projects Grant 14140902800 (to S.L.), National Key Research and Development Program Grant 2016YFC0900200, NIH Grant 1U54 CA199090-01 (to W.W. and J.R.H.), the Phelps Family Foundation (W.W.), and Shanghai Chest Hospital Grant 2014YZDC10600 (to S.L.).

1. Light RW (2002) Clinical practice. Pleural effusion. *N Engl J Med* 346(25):1971–1977.
2. Heffner JE (2008) Diagnosis and management of malignant pleural effusions. *Respirology* 13(1):5–20.
3. Porcel JM (2013) Pleural fluid biomarkers: Beyond the Light criteria. *Clin Chest Med* 34(1):27–37.
4. Krebs MG, et al. (2014) Molecular analysis of circulating tumour cells-biology and biomarkers. *Nat Rev Clin Oncol* 11(3):129–144.
5. Andree KC, van Dalum G, Terstappen LW (2016) Challenges in circulating tumor cell detection by the CellSearch system. *Mol Oncol* 10(3):395–407.
6. Hanahan D, Weinberg RA (2011) Hallmarks of cancer: The next generation. *Cell* 144(5):646–674.
7. Hensley CT, et al. (2016) Metabolic heterogeneity in human lung tumors. *Cell* 164(4): 681–694.
8. Dooms C, et al. (2009) Association between 18F-fluoro-2-deoxy-D-glucose uptake values and tumor vitality: Prognostic value of positron emission tomography in early-stage non-small cell lung cancer. *J Thorac Oncol* 4(7):822–828.
9. Millon SR, et al. (2011) Uptake of 2-NBDG as a method to monitor therapy response in breast cancer cell lines. *Breast Cancer Res Treat* 126(1):55–62.
10. O'Neil RG, Wu L, Mullani N (2005) Uptake of a fluorescent deoxyglucose analog (2-NBDG) in tumor cells. *Mol Imaging Biol* 7(6):388–392.
11. Tsytsarev V, et al. (2012) In vivo imaging of epileptic activity using 2-NBDG, a fluorescent deoxyglucose analog. *J Neurosci Methods* 203(1):136–140.
12. Yamada K, Saito M, Matsuoka H, Inagaki N (2007) A real-time method of imaging glucose uptake in single, living mammalian cells. *Nat Protoc* 2(3):753–762.
13. Langsner RJ, et al. (2011) Wide-field imaging of fluorescent deoxy-glucose in ex vivo malignant and normal breast tissue. *Biomed Opt Express* 2(6):1514–1523.
14. Sequist LV, et al. (2011) Genotypic and histological evolution of lung cancers acquiring resistance to EGFR inhibitors. *Sci Transl Med* 3(75):75ra26.
15. Han SW, et al. (2005) Predictive and prognostic impact of epidermal growth factor receptor mutation in non-small-cell lung cancer patients treated with gefitinib. *J Clin Oncol* 23(11):2493–2501.
16. Lynch TJ, et al. (2004) Activating mutations in the epidermal growth factor receptor underlying responsiveness of non-small-cell lung cancer to gefitinib. *N Engl J Med* 350(21):2129–2139.
17. Cristofanilli M, et al. (2004) Circulating tumor cells, disease progression, and survival in metastatic breast cancer. *N Engl J Med* 351(8):781–791.
18. Pecot CV, et al. (2011) A novel platform for detection of CK+ and CK- CTCs. *Cancer Discov* 1(7):580–586.
19. Travis WD, et al. (2011) International association for the study of lung cancer/american thoracic society/european respiratory society international multidisciplinary classification of lung adenocarcinoma. *J Thorac Oncol* 6(2):244–285.
20. Gandhi J, et al. (2009) Alterations in genes of the EGFR signaling pathway and their relationship to EGFR tyrosine kinase inhibitor sensitivity in lung cancer cell lines. *PLoS One* 4(2):e4576.
21. Bedrossian CW (1998) Diagnostic problems in serous effusions. *Diagn Cytopathol* 19(2):131–137.
22. Rashmi K, Shashikala P, Hiremath S, Basavaraj HG (2008) Cells in pleural fluid and their value in differential diagnosis. *J Cytol* 25(4):138–143.
23. Heffner JE (2010) Management of the patient with a malignant pleural effusion. *Semin Respir Crit Care Med* 31(6):723–733.
24. Saguil A, Wyrick K, Hallgren J (2014) Diagnostic approach to pleural effusion. *Am Fam Physician* 90(2):99–104.
25. Pantel K, Alix-Panabières C (2016) Functional studies on viable circulating tumor cells. *Clin Chem* 62(2):328–334.
26. Duysinx B, et al. (2008) Prognostic value of metabolic imaging in non-small cell lung cancers with neoplasic pleural effusion. *Nucl Med Commun* 29(11):982–986.
27. Wu SG, et al. (2013) Survival of lung adenocarcinoma patients with malignant pleural effusion. *Eur Respir J* 41(6):1409–1418.
28. Mok TS, et al. (2009) Gefitinib or carboplatin-paclitaxel in pulmonary adenocarcinoma. *N Engl J Med* 361(10):947–957.
29. Pao W, Ladanyi M (2007) Epidermal growth factor receptor mutation testing in lung cancer: Searching for the ideal method. *Clin Cancer Res* 13(17):4954–4955.